ACS APPLIED MATERIALS & INTERFACES

Research Article

Cite This: ACS Appl. Mater. Interfaces 2019, 11, 18849−18857

www.acsami.org

Support-Free Ceramic Stereolithography of Complex Overhanging Structures Based on an Elasto-viscoplastic Suspension Feedstock

Li He, Fan Fei, Wenbo Wang, and Xuan Song*

Department of Industrial and Systems Engineering, Center for Computer-Aided Design, The University of Iowa, Iowa City, Iowa 52242, United States

Supporting Information

ABSTRACT: Ceramic stereolithography (CSL) is an additive manufacturing method for creating ceramic three-dimensional (3D) objects via the layer-by-layer photopolymerization of a ceramic suspension. A key challenge in CSL is that support structures are required for building overhanging structures to prevent part damage or deformation caused by gravity or process-induced shears. Removing the support structures can result in issues such as poor surface quality, high risk of cracking, etc. To overcome this challenge, this article presents a new CSL-based ceramic fabrication method that uses an elasto-viscoplastic ceramic suspension as the feedstock material. The suspension's inherently strong interparticle resistive force can support overhangs without the need for building additional support structures; a temperature-controlled layer-coating module is designed to dynamically form a localized suspension bridge above the free surface of previously deposited materials, which allows for the application of fresh thin layers with a controlled shear force. The article presents material design and characterizations and discusses key process parameters and their effects on the geometry retention of fabricated overhangs. This new process provides the potential for fabricating ceramic 3D objects with complex overhangs, such as vascular networks, biomimetic heat exchangers, and microreactors.

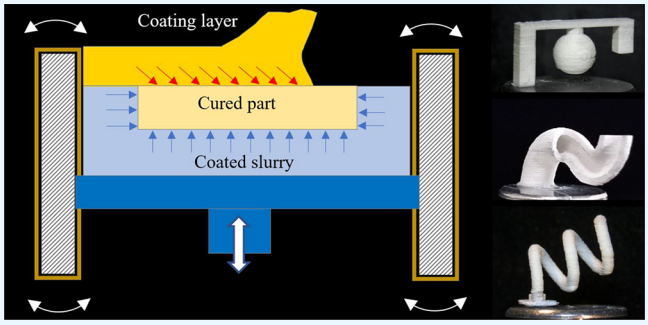

KEYWORDS: *ceramic stereolithography, overhang, support-free, elasto-viscoplasticity, suspension bridge*

1. INTRODUCTION

In the past decade, additive manufacturing (AM) of ceramics has gained importance in many industries,[1−5] thanks to its flexibility in achieving complex ceramic structures that are extremely difficult to produce with traditional machining methods because of the inherent brittleness of ceramics. Among the different AM approaches for ceramic fabrication, ceramic stereolithography (CSL) has been one of the most effective for creating high-accuracy and fully dense ceramics.[6] A typical CSL fabrication process is illustrated in Figure 1a: a computer-aided design (CAD) model is first sliced into a series of digital images; a thin layer of a slurry mixture comprising ceramic nanoparticles and photocurable resin is then coated by a doctor blade and cured via exposure to a sliced digital image; repeating this procedure layer by layer leads to a green part, which contains ceramic nanoparticles uniformly distributed in a cured resin matrix; afterward, the green part is heat-treated to decompose the polymer matrix and fuse ceramic nanoparticles into a dense ceramic component.

Although CSL can achieve ceramic components with relatively high accuracy and density in comparison to other ceramic AM processes, it has limited ability to construct 3D structures with complex overhangs, i.e., a feature not directly supported by underlying layers, as shown in Figure 1b−d. More specifically, when building an overhanging structure, CSL requires the generation of support structures underneath to protect the overhang from collapsing or deforming under gravity, and removing support structures can be costly. The added support structures not only require extra time to remove but also reduce the surface quality of the final parts. The surface defect resulting from the support removal contains many microcracks, which will propagate during the heat treatment and potentially lead to cracks and delamination of the green parts. The crack tip will also cause stress concentration when the component is under load, adversely affecting the mechanical properties of the final product and subsequently increasing the risk of failure.[7,8] Numerous research efforts have been carried out to build overhangs, such as the use of soluble support materials,[9−11] design optimization of support structures,[3,12] and multidirectional AM.[4,13] However, these methods either cannot entirely eliminate support structures or are too complicated to be attempted for CSL.

The aim of this paper is to present a new CSL-based AM method, called suspension-enclosing projection stereolithography (SEPS), to achieve support-free ceramic fabrication of

Received: March 8, 2019
Accepted: May 6, 2019
Published: May 6, 2019

DOI: 10.1021/acsami.9b04205
ACS Appl. Mater. Interfaces 2019, 11, 18849−18857

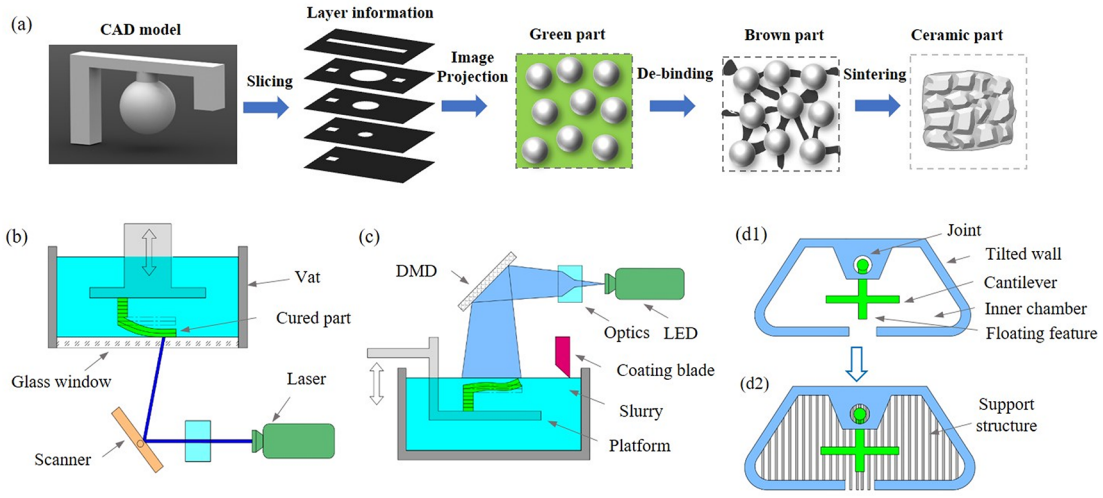

Figure 1. (a) Schematic of a typical CSL process; (b) schematic of a bottom-up CSL process; (c) schematic of a top-down CSL process; (d) schematic of a CAD model with typical overhang features (d1) and a green part printed with support structures (d2).

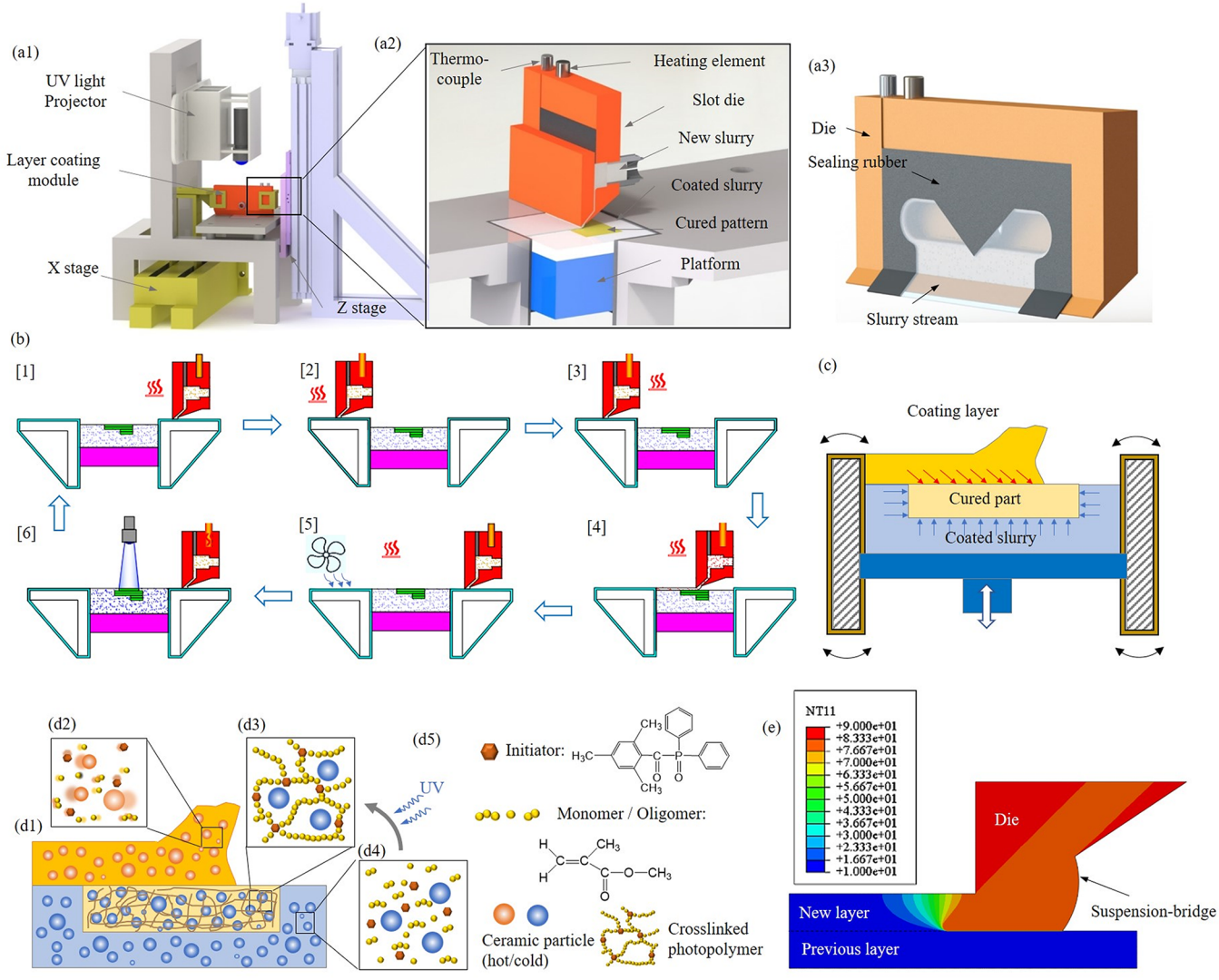

Figure 2. (a) Schematic representation of the SEPS process; (b) fabrication procedures of one layer; (c) supporting mechanism; (d) different ingredients of an elasto-viscoplastic ceramic suspension; (e) simulation of temperature distribution in the suspension bridge.

DOI: 10.1021/acsami.9b04205
ACS Appl. Mater. Interfaces 2019, 11, 18849−18857

complex overhangs. It utilizes the inherently strong interparticle resistive force of an elasto-viscoplastic feedstock suspension to protect the overhangs against damage or deformation without the need to build additional support structures. A suspension-bridge-based layer-recoating strategy is developed to accurately deposit thin layers of an elasto-viscoplastic suspension feedstock with a controlled shear force.

2. EXPERIMENTAL SECTION

2.1. Material Preparation. The feedstock used in the SEPS process is an elasto-viscoplastic ceramic suspension, which is a mixture of fine ceramic particles and a liquid photopolymer resin. In this research, aluminum oxide (α-Al_2O_3, CR1, Baikowski, Charlotte, USA) was used as a model material. The powder possesses a bulk density of 0.6 g/cm^3 and a true density of 3.99 g/cm^3 at 20 °C. The D10, D50, D90 values of the powder are 0.7, 1.0, and 2.5 μm, respectively. In addition to alumina, other ceramic particles (e.g., zirconium oxide and calcium phosphate) that can form a desired elasto-viscoplastic suspension can be used. The photopolymer resin used in the research is a commercial photocurable resin (FLGPCL01, Formlabs, Boston, USA). The resin contains more than 99 wt % methacrylated monomer/oligomer and less than 1 wt % diphenyl (2,4,6-trimethylbenzoyl) phosphine oxide as a photoinitiator. The density of the resin is 1.09−1.12 g/cm^3.

For the preparation of an elasto-viscoplastic ceramic suspension, as-received aluminum oxide powder was first manually mixed with the photopolymer resin with different particle volume fractions varying from 3 vol % to 40 vol %. A dispersant (phosphate ester, PS-131, AkzoNobel, Amsterdam, Netherlands) was added in the suspension with a concentration of 0.8 wt %. After that, the materials were further mixed in a ball mill machine for 2 h at a speed of 300 rpm. The mixed slurry was then degassed three times (10 min per time) in a vacuum of −1.5 bar. Because no low-viscosity solvent was added to the mixture as a diluent, the achieved ceramic suspensions exhibit extremely high viscosity as well as an obvious solid-like behavior.[14,15]

2.2. Fabrication System. A schematic representation of the proposed SEPS process is given in Figure 2a. The fabrication system consists of a customized light engine, a temperature-controlled layer-recoating module, a cooling building platform sliding in an enclosing chamber, and X/Z stages. The light engine projects digital images with a wavelength of 405 nm via a digital micromirror device (DMD) (Texas Instruments). The layer-recoating module is a customized slot die with an inclined lip, as shown in Figures 2a-2, a-3, and is used to recoat a thin layer of an elasto-viscoplastic ceramic suspension on top of previous layers. The temperature of the layer-recoating module is controlled through a heating element and a thermocouple. Compared to conventional slot die coating,[16,17] this modified recoating method can achieve layer recoating of high-viscosity materials at a controlled shear force. The side walls of the enclosing chamber are each wrapped by a flexible belt moving with the building platform. A low temperature (e.g., 0−20 °C) is maintained in previously deposited ceramic suspensions through a cooling fan and a semiconductor chilling plate mounted under the building platform.

2.3. Printing Procedures. The fabrication procedures of the SEPS process are described in Figure 2b. Upon fabrication initialization of one layer, the following steps occur: (1) the building platform moves down a distance of nd ($n > 1$, and d is the layer thickness); (2) the layer-recoating module moves to the left and prepares for recoating a new layer; (3) the building platform moves up a distance of $(n - 1)d$ along with the cured layers and uncured slurries; (4) the layer-recoating module moves to the right and delivers a uniform slurry layer at a predefined temperature into the volume enclosed by the chamber and previous layers; (5) the cooling fan and the semiconductor chilling plate are turned on to reduce the temperature of a slurry layer once delivered; and (6) the light engine is activated to project a digital image onto the fresh slurry surface to cure a new layer. The photopolymerization process involved in the curing of a new layer is explained in Figure S1. These steps are repeated until the whole component is completed.

2.4. Material Rheology Characterization. Rheological properties of elasto-viscoplastic ceramic suspensions were measured using a rheometer (Anton Paar MCR 72, Ashland, VA, USA). All measurements were carried out using a plate−plate measurement geometry (PP25 with a diameter of 25 mm), a 1 mm measure gap width, and under a temperature of 20 °C unless otherwise noted. The viscosity of suspensions with volume fractions from 3 to 40 vol % was measured under a shear rate from 0.1 to 1000 s^{-1} to investigate the effects of solid loading and operation speed on the flowability of the materials. Frequency sweeps were performed with an angular frequency varying from 1 to 100 rad/s and a fixed shear strain of 0.1% to characterize the time-dependent rheological behaviors of the suspensions. After that, amplitude sweeps were measured under a temperature between 0 and 80 °C at a fixed angular frequency ω = 100 rad/s. Apparent yield stress and yield strain were determined as the intersection point between elastic modulus and loss modulus in these measurements. Shear stress of suspensions was measured at a shear rate ranging from 0.01 to 100 s^{-1} and a temperature between 0 and 80 °C to determine layer-recoating-induced shear forces under different recoating speeds.

2.5. Analysis of New Layer Application. New layer recoating during the SEPS process was monitored by a camera integrated in the SEPS machine. Application of a new layer via the recoating module was analyzed, including the formation of a suspension bridge and spreading of a thin fresh layer. A ceramic suspension of 30 vol % was selected to perform the analysis due to its excellent rheological behaviors suitable for the SEPS process. The layer-recoating module was moved at a speed of 1 mm/s across the building platform and extruded the suspension at an extrusion speed of 5 μL/s into a layer with a thickness of 0.1 mm. The temperature of the layer-recoating module was set to 20 °C, and that of the building platform and previously deposited suspensions was set to 10 °C.

2.6. Overhang Stability Test. The influences of new layer recoating on the stability of overhangs were investigated. Shifting distances of overhanging features subjected to layer-recoating-induced shears were measured as a function of overhang size and setting temperatures of the layer-recoating module. Square overhanging features (sizes varying from 100 to 0.25 mm^2 and a thickness of 0.1 mm) were first printed on the free surface of previously deposited suspensions. The temperature of previously deposited suspensions in the chamber was set to 10 °C. The layer-recoating module was heated to 20, 40, 60, and 80 °C and used to deliver new layers on top of the overhanging features. Shifting distances of the overhanging features were recorded.

3. RESULTS AND DISCUSSION

3.1. Supporting Mechanism. Support-free fabrication of ceramics via the SEPS process is enabled by the temperature-dependent rheological behaviors of an elasto-viscoplastic ceramic suspension feedstock. That is, an overhang submerged in a cold ceramic suspension undergoes a uniform resistive force from the suspension surrounding it, which counteracts gravitational and process-induced shear forces imposed on the overhang. The overhang can be held in position when a balance is achieved among the forces, as shown in Figure 2c. With a constant gravitational force for a given overhang, the supporting resistive force can be tailored by changing the temperature of the ceramic suspension feedstock, and process-induced shear forces can be carefully controlled through a suspension-bridge-based layer-recoating strategy.

Process-induced shear forces in a conventional CSL process mainly stem from wall boundary slip and new layer recoating. In the SEPS process, wall-boundary-induced shear forces can be negligible thanks to the use of rotating belts wrapped on the enclosing chamber walls, which move together with the suspension and introduce no velocity gradient. Layer-recoating-induced shear forces are minimized by locally

DOI: 10.1021/acsami.9b04205
ACS Appl. Mater. Interfaces 2019, 11, 18849−18857

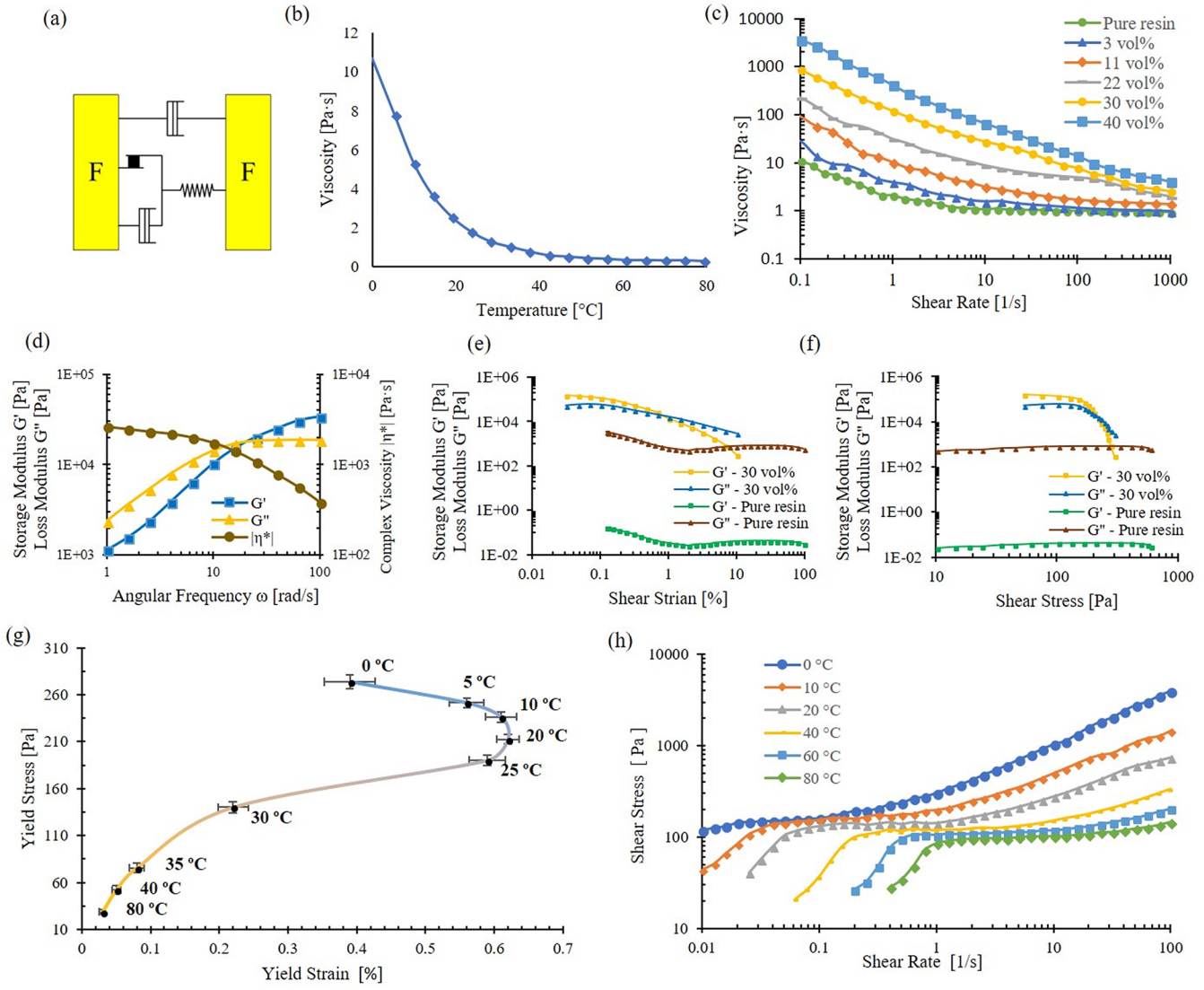

Figure 3. (a) Mechanical analogue for an elasto-viscoplastic ceramic suspension used in the SEPS process; (b) the viscosity of pure resin at different temperatures from 0 to 80 °C (at a shear rate of 10 s^{-1}); (c) the viscosity of suspensions with different volume fractions of ceramics varying from 0 to 40 vol %; (d) frequency sweep testing results of a 30 vol % suspension at a shear strain γ = 0.1%; amplitude sweep test at angular frequency ω = 100 rad/s with (e) shear strain and (f) shear stress as the x-axis; (g) yield points and (h) shear stress of a 30 vol % slurry at different temperatures.

forming a suspension bridge between the layer-recoating module and the building platform and accurately tailoring a temperature gradient across the suspension bridge. The suspension bridge was created via a customized recoating die with a specially designed inclined die lip (refer to Figure 2a-2). With such a recoating design, a suspension exiting the lip flows in the direction opposite of the moving direction of the coating die, achieving an overall flow speed of zero at the interface between the suspension bridge and previously deposited layers and thus inducing no additional shear force on the overhang. On the other hand, a temperature gradient builds up across the suspension bridge by heating the top end in the layer-recoating module and cooling the bottom end merging with previous layers (refer to Figure 2e). A higher temperature at the top end enables a reduced shear force on an overhang as the suspension bridge is spread into a thin layer, due to a significantly reduced viscosity of the resin vehicle (refer to Figure 3b), an increased particle mobility along the streamline and thus a decreased degree of interparticle friction;[18−20] a low temperature at the bottom end of the suspension bridge enables a high supporting resistive force from the suspension onto an overhang once it is coated into a thin layer on top of previously deposited layers.

3.2. Material Rheology. A suspension feedstock suitable for achieving support-free overhang fabrication via the SEPS process is desired to simultaneously exhibit thixotropy, viscoelasticity, and yielding behaviors, the combination of which is known as elasto-viscoelasticity. An elasto-viscoplastic material behaves like a solid when an external shear force is under a critical value, i.e., yield stress τ_y, and flows like liquid when the shear force is less than the yield stress. This behavior can be illustrated by Saramito's mechanical analogue model[21−23] as depicted in Figure 3a, where the spring represents the elastic element, the dashpots describe the viscous stress, and the friction element describes the yield stress of the material. To identify the optimal material and operation combination for the SEPS process, ceramic

DOI: 10.1021/acsami.9b04205
ACS Appl. Mater. Interfaces 2019, 11, 18849−18857

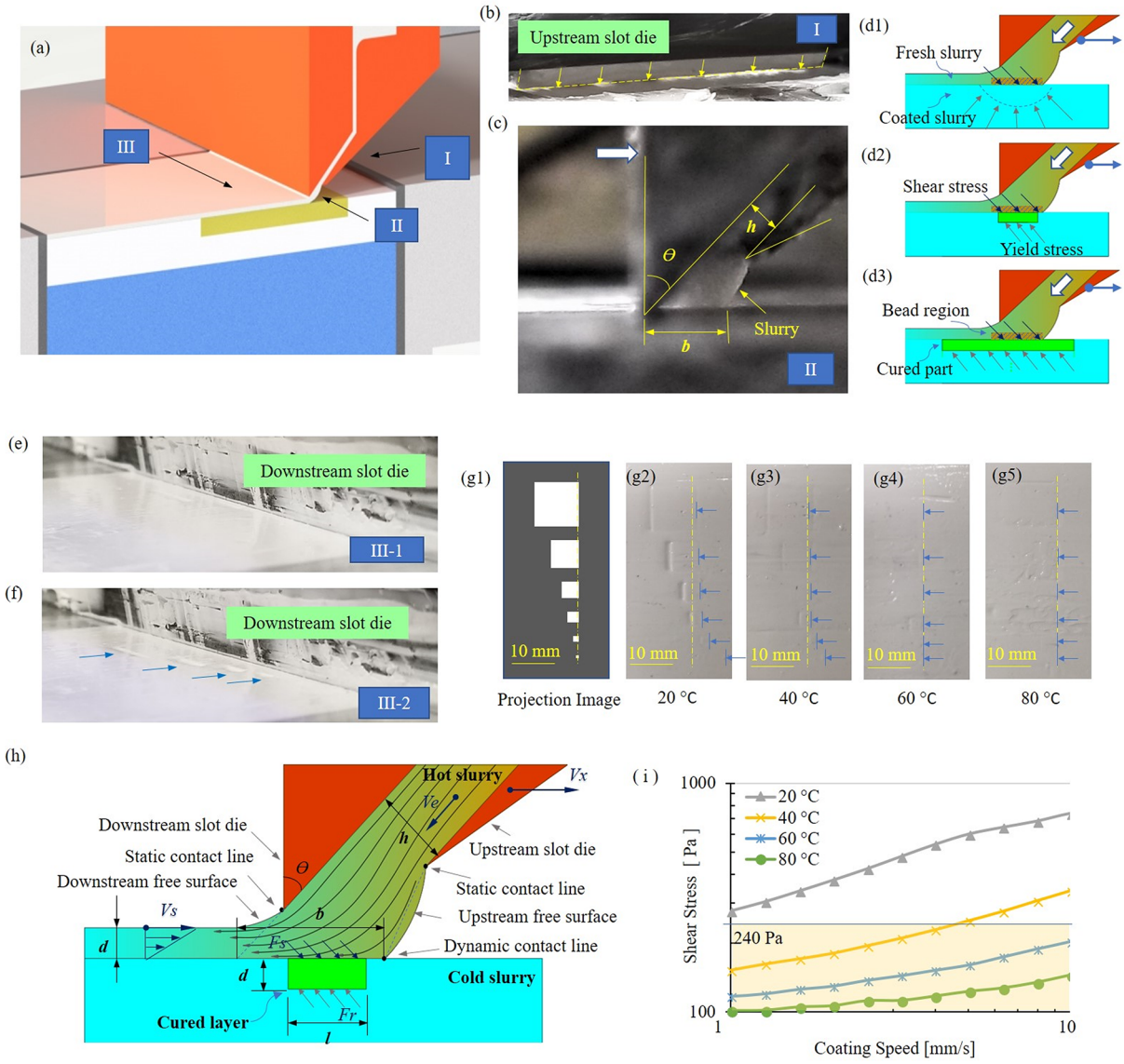

Figure 4. (a) Section view of the layer-recoating procedure; (b) formation of a uniform slurry extrusion stream along the die lip; (c) formation of a stable suspension bridge; (d) illustration of three coating conditions: only above the slurry (d1), above a small overhang piece (d2), and above a big overhang piece (d3); (e) new layer coated behind the module; (f) shifting of overhangs behind the recoating module; (g) dimensions and original positions of overhangs (g1) and shifting distances of different overhangs under a heating temperature of 20 to 80 °C (g1−g5); (h) illustration of design parameters of the suspension-bridge-based layer recoating; (i) shear stress versus coating speed under different heating temperatures.

suspensions with different solid loadings and processing temperatures were examined.

The flowability of pure resin and ceramic suspensions with different solid loadings are shown in Figure 3b, c and Figure S2. In Figure 3b, the pure methacrylate-based resin displays a dramatic decrease in viscosity (measured at a shear rate of 10 s^{-1}), as the temperature increases from 0 to 80 °C. In Figure 3c, as alumina particles were added into the resin, the viscosity of the suspensions increases with an increasing solid loading, which is mainly attributed to the increasing interparticle forces (particularly the friction). As the volume fraction of ceramics further increases to 40 vol % or above, the interparticle friction gradually dominates the flow behaviors of the suspensions, and the viscosity becomes extremely high, which consequently requires a high extrusion force and may easily result in air entrainment. Meanwhile, all the tested materials exhibit a desired thixotropic behavior at room temperature, assuring smooth extrusion. In the following study, a volume fraction of 30 vol % was selected, which exhibits a complex viscosity $|\eta^*|$ greater than 2.6 kPa s (room temperature) at a low sweep frequency <10 rad/s (refer to Figure 3d), indicating a low flowability at low shear rates suitable for supporting overhangs. It should be noted that a higher volume fraction of ceramics may be applicable through adjusting the rheological properties of the suspension by optimizing the ingredients of the material, such as the concentration of dispersant, pH value, a diluent additive, etc.

The viscoelasticity and yielding behaviors of the selected 30 vol % suspension are presented in Figure 3d−f. At a low sweep frequency <10 rad/s, the loss modulus (G'') of this material is greater than its storage modulus (G'), which indicates a viscous behavior of the material and susceptibility to

DOI: 10.1021/acsami.9b04205
ACS Appl. Mater. Interfaces 2019, 11, 18849−18857

segregation at low shear rates. As the sweep frequency increases, G' exceeds G'', and an elastic behavior is identified, which allows for stable particle dispersion during layer recoating. The yield stress (τ_y) of the suspension is determined as 210 Pa under ambient temperature at the crossover point between the two moduli curves in Figure 3e, f, after which the suspension undergoes a solidlike-to-liquidlike transition.[24,25] In comparison, the G'' curve of the pure resin is higher than G' over the entire amplitude spectrum, which indicates an absence of a yielding behavior with the resin.

The temperature dependence of rheological behaviors of the 30 vol % ceramic suspension is given in Figures 3g, h. The measurement of each yield point in Figure 3g was repeated 4 times. More complete data can be found in Figures S4 and S5. Figure 3g reveals that the yield stress τ_y of this material decreases from 260 to 20 Pa as the temperature increases from 0 to 80 °C; the yield strain ε_y increases with an increasing temperature less than 20 °C but starts to decrease as the temperature continues increasing after 20 °C. This behavior is mainly caused by the temperature-dependent rheology of the resin vehicle and the varying interparticle friction at different temperatures. Since a higher yield stress (240−260 Pa) of the material is achieved in the temperature range of 0−10 °C, we selected 10 °C as the cooling temperature of the building platform to attain the optimal supportability of the material for overhangs. Moreover, as shown in Figure 3h and Figure S5, the shear stress induced in the material decreases to 110 Pa or lower as the temperature increases to 80 °C, which is well below the yield point 240 Pa of the material at 10 °C. Such a property allows for a careful control of shear force induced by layer recoating of the material on overhangs.

3.3. Formation of a Stable Suspension Bridge for Layer Recoating. As a ceramic suspension is extruded through the inclined die lip (lip angle Θ and gap h) of the layer-recoating module, as shown in Figure 4a, a uniform stream forms across the lip and instantaneously swells outward on the upstream free surface due to the relaxation of the polymer within the flow stream, resulting in a convex suspension bridge between the lip and the free surface of previously deposited layers (refer to Figure 4b, c and Figure S6). A schematic illustration of the formed suspension bridge is shown in Figure 4h. It has been experimentally determined that the suspension bridge can maintain a stable shape under a controlled extrusion speed v_e and slot die velocity v_x; meanwhile, as an extruded material in the formed suspension bridge merges with previously deposited layers, it induces a shear force onto a zone with a fixed length $b \approx \frac{1.5h}{\cos\theta}$ (refer to Figure 4d). After the extruded suspension settles on the free surface, it is immediately spread by the downstream slot die tip, which was remodeled from a doctor blade, into a thin layer with no defect such as ribbing, rivulets, barring, and air entrainment,[26] as shown in Figure 4e.

3.4. Investigation of the Suspension/Overhang Interactions. A shear force induced by the extruded suspension on previously deposited layers during new layer recoating can shift an overhang from its original position, leading to the failure of the fabrication, as shown in Figure 4f. According to the overhang stability test, six overhanging pieces printed in the previous layer with a size of 100 mm^2 to 0.25 mm^2 and a thickness of 0.1 mm were dragged away from their original positions for different shifting distances. The shifting distances are marked in Figures 4g-2−g-5, where the yellow dashed line represents the original position and the blue line represents the final position after new layer recoating. With a constant cooling temperature of 10 °C on the building platform, the shifting distances are dependent on the overhang size and heating temperature of the layer-recoating module. Under the same heating temperature, a larger overhang shifted a smaller distance due to a greater resistance from the suspension surrounding it. When the heating temperature was increased from 20 to 80 °C, the shifting distances were gradually reduced. At a heating temperature higher than 60 °C, no evident shifting can be observed, even with the smallest overhang (refer to Figures 4g-4, g-5).

3.5. Effects of Process Parameters and Overhang Size. To analyze the effects of process parameters and overhang size on the fabrication, we assume that the fluid in the suspension bridge is a laminar flow with a mean speed of v_e, as described in Figure 4e. To hold an overhang in position, the flow velocity at the interface between the suspension bridge and previously deposited layers must be zero. Assume the flow speed at the free surface of the newly coated layer is v_s. We then have

$$v_s = v_x - v_{ex} = v_x - v_e \sin\theta \tag{1}$$

where v_x is the moving speed of the layer-recoating module, and v_{ex} is the extrusion speed along the recoating direction. The speed gradient $0 \sim v_s$ across the new layer thickness d leads to a shear rate $\dot{\gamma}$ on the new layer, and

$$\dot{\gamma} = v_s/d \tag{2}$$

According to the law of mass conservation, we also have

$$v_e h = v_x d \tag{3}$$

On the basis of eqs 1−3, we obtain

$$\tau_s = \eta\dot{\gamma} = \eta v_x\left(\frac{1}{d} - \frac{1}{h}\sin\theta\right) \tag{4}$$

where η is the apparent viscosity.

To ensure that an overhang with a length l is held in position by the surrounding suspension, the total shear force F_s must satisfy

$$F_s < F_{r,max} \tag{5}$$

where $F_{r,max}$ is the maximum resistive force from the suspension prior to the yield point, and $F_{r,max} = \tau_y l$ (in the 2D case). Because a new layer was cooled down immediately after it was deposited, we ignored the thermal transport between a newly deposited layer and previous layers, and assume the temperature of the newly deposited layer was the same as the previous layers in the enclosing chamber. Thus, the value of τ_y of the surrounding suspension can be directly obtained from the experimental results in Figure 3g. For the ineq (5), two cases may occur with different overhang size l:

Case 1: if $\tau_s \le \tau_y$, ineq 5 will always hold. Then an overhang with any $l > 50$ μm will be kept in position during the layer recoating. Fifty micromters is the resolution of our current system.

Case 2: if $\tau_s > \tau_y$, two conditions need to be considered:

(i) if $l < b$, as shown in Figure 4d-2, the shear force F_s is always greater than the maximum yield force, i.e., $F_s = \tau_s l > F_{ymax} = \tau_y l$, and the overhang cannot be successfully fabricated without building support structures.

DOI: 10.1021/acsami.9b04205
ACS Appl. Mater. Interfaces 2019, 11, 18849−18857

Figure 5. Fabrication results via the SEPS process: (a) a structure with an overhanging ball and cube; (b) a tube with an inner overhanging chamber; (c) a spring structure printed with an upward slope angle; (d) a ball check valve with an inner chamber and a movable ball inside printed without assembly; (e) a heat exchanger with an inner chamber and overhanging hollow pipeline (e1−e3); (f) a combustion chamber with overhanging nozzles (f1−f3); (g) a CAD model of a treelike structure (g1) and the printed treelike structure and its microstructures (g2−g6); (h1, h2) the sintered overhanging tube; (i1, i2) the sintered combustion chamber.

(ii) If $l \geq b$, as shown in Figure 4d-3, $F_s = \tau_s b$, the inequation below should hold:

$$\tau_s b \leq \tau_y l \tag{6}$$

Plugging eq 4 and $b \approx \frac{1.5h}{\cos\theta}$ into (6), we have

$$l \geq \frac{1.5h\eta v_x\left(\frac{1}{d} - \frac{1}{h}\sin\theta\right)}{\tau_y \cos\theta} = l_{\min} \tag{7}$$

where $l_{\min}$ suggests the minimum overhang size that can be printed in this case.

Therefore, to enable support-free fabrication of an overhanging structure with high accuracy, it is desired to control the shear stress from the suspension bridge to be less than the yield stress of the coated suspension. Prior testing results show that the yield stress of a 30 vol % suspension in the enclosing chamber at 10 °C is measured as 240 Pa. According to the shear stress test results shown in Figure 4i, it is obvious that reducing the recoating speed and increasing the heating temperature of the layer-recoating module can restrict the induced shear stress in a desired regime of operation (τ_s < 240 Pa). Any shear stress test points below the threshold of 240 Pa can satisfy the requirement of support-free fabrication without a limitation in the overhang size.

3.6. Fabrication Results of Overhanging Structures.

Several test cases were printed via the SEPS process with a 30 vol % alumina suspension and a layer thickness d = 100 μm. The layer-recoating module was designed with h = 0.5 mm to provide a sufficient die gap for smooth extrusion and enable a relatively small suspension bridge. In addition, the lip angle θ was 45°, which is the tip angle of the doctor blade mounted at the downstream of the slot die. During printing, the slot die was heated to 80 °C, and the platform was cooled to 10 °C. The recoating speed v_x was set to 5 mm/s.

First, a classic overhanging structure was printed as shown in Figure 5a. During the fabrication, the very bottom layers of the overhanging ball and cube were directly printed on previously deposited suspensions without building any support structures underneath. The fabrication result of this model demonstrates that the SEPS process did not generate any macroscopic deformation or shifting in the layers that were stacked directly on the suspension. A tube sample in Figure 5b shows that a curved channel with a downward-facing surface can be printed without support structures. A spring model in Figure 5c

DOI: 10.1021/acsami.9b04205
ACS Appl. Mater. Interfaces 2019, 11, 18849−18857

indicates the feasibility of printing complex, tiny, curved features, which are always difficult to build with conventional CSL due to the risk of damage caused by support structure removal. The check valve assembly in Figure 5d shows the possibility of fabricating several assembled pieces as a single, assembly free object via the SEPS process. Normally, a ball check valve requires designing the body in two halves to allow for postmanufacturing assembly of the movable ball. With the SEPS process, the assembly can be achieved after cleaning the uncured slurry inside the tube in alcohol with an ultrasonic cleaner.

A heat exchanger model with a complex inner overhanging pipeline and a wide cover was printed, as shown in Figure 5e-1−e-3. The multiscale inner channels and overhanging pipeline can be fabricated integrally via the SEPS process. Furthermore, a combustion chamber was printed as given in Figure 5f-1−f-3. This chamber design has inner overhanging structures in a millimeter range along all potential building orientations, which makes it extremely challenging to build using existing CSL processes. Our SEPS process can easily create this model without using any support structure. A tree-like 3D model was fabricated and presented in Figure 5g-1−g-6. It features arbitrarily orientated branches in 3D space. This complex, tiny truss structure cannot be effectively built by simply adding support structures because the branches can be easily broken when removing support. The fabrication results of such treelike structures indicate the promising prospects of the SEPS process in complex support-free vascular structure production, such as nature-inspired heat exchangers[27] and blood vessel networks.[28,29] Two green parts, including the overhang tube and the combustion chamber, were further debinded and sintered. The debinding and sintering temperature curves are given in Figure S7. The sintered parts are shown in Figure 5h, i, which experienced an average shrinkage of 25% along each direction. The density of the parts was measured as 90% ± 2% of the true density by Archimedes' method.

4. CONCLUSIONS

This paper presents a support-free CSL-based AM process called SEPS, which utilizes an elasto-viscoplastic ceramic suspension as the feedstock to eliminate the need for support structures for building overhanging features. Material properties and process parameters required for support-free fabrication via the SEPS process have been discussed. According to the experimental results, a lower temperature (e.g., 10 °C) of a suspension deposited on the building platform can offer stable supportability; a lower coating speed and a higher heating temperature (e.g., 80 °C) of the layer-recoating module enable a shear stress that is sufficiently low (<240 Pa) to not drag away cured overhang features. Experimental and analytical studies were performed on a suspension-bridge-based layer-recoating strategy based on a customized slot die module with an inclined die lip. The fabrication results of several test cases verified the potential of the presented SEPS process in achieving complex ceramic overhanging components such as vascular networks, biomimetic heat exchangers, microreactors, etc.

In the future, a finer layer thickness and better recoating quality will be achieved by improving the accuracy of the layer-coating module. A lower heating temperature of the layer-recoating module will be investigated to avoid thermal curing of the suspension after long-term heating. Moreover, thermal transfer during the suspension-overhang interaction will be numerically and experimentally studied. In addition, process parameters, material properties, and slot die design will be further optimized to achieve the lowest energy consumption.

■ ASSOCIATED CONTENT

Supporting Information

The Supporting Information is available free of charge on the ACS Publications website at DOI: 10.1021/acsami.9b04205.

Detailed information on materials, rheological properties, the suspension-bridge-based layer recoating, and post-processing (PDF)

■ AUTHOR INFORMATION

Corresponding Author

*Email: xuan-song@uiowa.edu.

ORCID

Xuan Song: 0000-0002-7353-4252

Notes

The authors declare no competing financial interest.

■ ACKNOWLEDGMENTS

This work was partially supported by the National Science Foundation (NSF) Grant CMMI-1825962.

■ REFERENCES

(1) Chen, Z.; Song, X.; Lei, L.; Chen, X.; Fei, C.; Chiu, C. T.; Qian, X.; Ma, T.; Yang, Y.; Shung, K.; et al. 3d Printing of Piezoelectric Element for Energy Focusing and Ultrasonic Sensing. *Nano Energy* **2016**, *27*, 78−86.

(2) Song, X.; Chen, Y.; Lee, T. W.; Wu, S.; Cheng, L. Ceramic Fabrication Using Mask-Image-Projection-Based Stereolithography Integrated with Tape-Casting. *J. Manuf. Processes.* **2015**, *20*, 456−464.

(3) Vanek, J.; Galicia, J. A. G.; Benes, B. In *Clever Support: Efficient Support Structure Generation for Digital Fabrication, Computer graphics forum.*; Wiley Online Library: 2014; pp 117−125.

(4) Wu, C.; Dai, C.; Fang, G.; Liu, Y.-J.; Wang, C. C. In RoboFDM: A Robotic System for Support-Free Fabrication Using FDM. *2017 IEEE International Conference on Robotics and Automation (ICRA)*; IEEE: 2017; pp 1175−1180.

(5) Song, X.; Chen, Z.; Lei, L.; Shung, K.; Zhou, Q.; Chen, Y. Piezoelectric Component Fabrication Using Projection-Based Stereolithography of Barium Titanate Ceramic Suspensions. *Rapid Prototyp. J.* **2017**, *23* (1), 44−53.

(6) Halloran, J. W. Ceramic Stereolithography: Additive Manufacturing for Ceramics by Photopolymerization. *Annu. Rev. Mater. Res.* **2016**, *46* (1), 19−40.

(7) Wang, L.; Aldinger, F. Near□Net Shape Forming of Advanced Ceramics. *Adv. Eng. Mater.* **2000**, *2* (3), 110−113.

(8) Zhang, Q.; Zhang, F.; Medarametla, S. P.; Li, H.; Zhou, C.; Lin, D. 3d Printing of Graphene Aerogels. *Small* **2016**, *12* (13), 1702−1708.

(9) Jin, J.; Chen, Y. Highly Removable Water Support for Stereolithography. *J. Manuf. Processes.* **2017**, *28*, 541−549.

(10) Priedeman, W. R., Jr.; Brosch, A. L., Soluble Material and Process for Three-Dimensional Modeling U.S. Patent 6790403B1, 2004.

(11) Zhang, W.; Leu, M. C.; Ji, Z.; Yan, Y. Rapid Freezing Prototyping with Water. *Mater. Eng.* **1999**, *20* (2), 139−145.

(12) Wang, W.; Liu, Y.-J.; Wu, J.; Tian, S.; Wang, C. C.; Liu, L.; Liu, X. Support-Free Hollowing. *IEEE Trans. Visual Comput. Graphics.* **2018**, *24* (10), 2787−2798.

(13) Song, X.; Pan, Y.; Chen, Y. Development of a Low-Cost Parallel Kinematic Machine for Multidirectional Additive Manufacturing. *J. Manuf. Sci. Eng.* **2015**, *137* (2), 021005−021005−13.

DOI: 10.1021/acsami.9b04205
ACS Appl. Mater. Interfaces 2019, 11, 18849−18857

(14) Larson, R. G. *The Structure and Rheology of Complex Fluids (Topics in Chemical Engineering).*; Oxford University Press: New York, 1999; Vol. *86*, p 108.
(15) He, L.; Song, X. Supportability of a High-Yield-Stress Slurry in a New Stereolithography-Based Ceramic Fabrication Process. *JOM* **2018**, *70* (3), 407−412.
(16) Kistler, S. F.; Schweizer, P. M. *Liquid Film Coating: Scientific Principles and Their Technological Implications.*; Springer: 1997; p 401−536.
(17) Cohen, E. D.; Gutoff, E. B. *Modern Coating and Drying Technology.*; VCH: New York, 1992; Vol. *1*.
(18) Tarì, G.; Olhero, S. M.; Ferreira, J. M. F. Influence of Temperature on Stability of Electrostatically Stabilized Alumina Suspensions. *J. Colloid Interface Sci.* **2000**, *231* (2), 221−227.
(19) Seal, A.; Chattopadhyay, D.; Sharma, A. D.; Sen, A.; Maiti, H. S. Influence of Ambient Temperature on the Rheological Properties of Alumina Tape Casting Slurry. *J. Eur. Ceram. Soc.* **2004**, *24* (8), 2275−2283.
(20) Uchikoshi, T.; Sakka, Y. Phosphate Esters as Dispersants for the Cathodic Electrophoretic Deposition of Alumina Suspensions. *J. Am. Ceram. Soc.* **2008**, *91* (6), 1923−1926.
(21) Fraggedakis, D.; Dimakopoulos, Y.; Tsamopoulos, J. Yielding the Yield-Stress Analysis: A Study Focused on the Effects of Elasticity on the Settling of a Single Spherical Particle in Simple Yield-Stress Fluids. *Soft Matter* **2016**, *12* (24), 5378−5401.
(22) Saramito, P. A New Constitutive Equation for Elastoviscoplastic Fluid Flows. *J. Non-Newtonian Fluid Mech.* **2007**, *145* (1), 1−14.
(23) De Souza Mendes, P. R. Thixotropic Elasto-Viscoplastic Model for Structured Fluids. *Soft Matter* **2011**, *7* (6), 2471−2483.
(24) Shih, W. Y.; Shih, W. H.; Aksay, I. A. Elastic and Yield Behavior of Strongly Flocculated Colloids. *J. Am. Ceram. Soc.* **1999**, *82* (3), 616−624.
(25) Compton, B. G.; Lewis, J. A. 3d□Printing of Lightweight Cellular Composites. *Adv. Mater.* **2014**, *26* (34), 5930−5935.
(26) Sartor, L. Slot Coating: Fluid Mechanics and Die Design. *PhD Thesis*; University of Minnesota: Minneapolis, MN, 1990; pp 5467−5467.
(27) Huang, Z.; Hwang, Y.; Radermacher, R. Review of Nature-Inspired Heat Exchanger Technology. *Int. J. Refrig.* **2017**, *78*, 1−17.
(28) Miller, J. S. The Billion Cell Construct: Will Three-Dimensional Printing Get Us There? *PLoS Biol.* **2014**, *12* (6), No. e1001882.
(29) Ionita, C. N.; Mokin, M.; Varble, N.; Bednarek, D. R.; Xiang, J.; Snyder, K. V.; Siddiqui, A. H.; Levy, E. I.; Meng, H.; Rudin, S. Challenges and Limitations of Patient-Specific Vascular Phantom Fabrication Using 3d Polyjet Printing. In *Medical Imaging 2014: Biomedical Applications in Molecular, Structural, and Functional Imaging.*; International Society for Optics and Photonics: 2014; p 90380M.

DOI: 10.1021/acsami.9b04205
ACS Appl. Mater. Interfaces 2019, 11, 18849−18857